ARR No. L4I11b

39p.

NATIONAL ADVISORY COMMITTEE FOR AERONAUTICS

WARTIME REPORT

ORIGINALLY ISSUED

September 1944 as
Advance Restricted Report L4I11b

HIGH-ALTITUDE COOLING

III - RADIATORS

By Jack N. Nielsen

Langley Memorial Aeronautical Laboratory
Langley Field, Va.

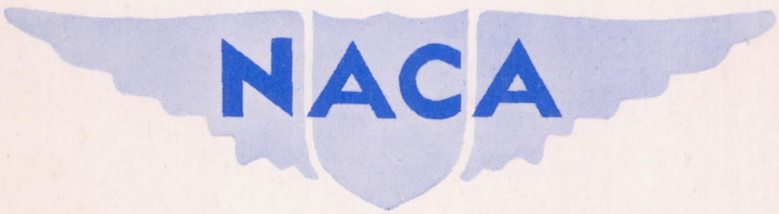

WASHINGTON

NACA ARR No. L4I11b

NATIONAL ADVISORY COMMITTEE FOR AERONAUTICS

ADVANCE RESTRICTED REPORT

HIGH-ALTITUDE COOLING

III - RADIATORS

By Jack N. Nielsen

SUMMARY

A detailed analysis has been made to take account of the high cooling-air velocity occurring in high-altitude radiators. Methods are developed for determining the heat-transfer rate, the pressure drop, and the drag power. Some effects of Mach number are shown. Radiator performance charts based on the analysis are presented for a wide range of the design variables. The application of the charts is shown by an example.

The performance charts show that the heat-transfer rate for a given total-pressure loss is not greatly affected by the high airplane velocities but that the necessary total-pressure loss and the resulting drag are both greatly increased at high altitudes.

INTRODUCTION

Extensive literature is available relative to the performance of ethylene-glycol radiators in the normal range of operating conditions. At high altitudes, however, certain effects that normally receive but little consideration acquire increased importance as a result of the high velocities of the cooling air through the tubes. The purpose of this paper is to describe and evaluate these effects.

The theories are outlined on which are based the calculations of heat transfer, of friction pressure drop, and of acceleration pressure drop at high Mach numbers. A general differential equation for the pressure drop and some approximate solutions for the equation are given. Radiator design charts based on the simplest of these approximate solutions are included. These charts

show, for a range of altitude up to 50,000 feet, the variation of heat dissipation per unit frontal area with pressure drop as well as the corresponding drag power. An example showing the use of the charts is also included.

This paper is the third of the series on high-altitude cooling. (See reference 1.)

SYMBOLS

V airspeed, feet per second

$\bar{V}$ mean flow velocity in radiator tube, feet per second

L radiator-tube length, feet

D radiator-tube diameter, feet

A cross-sectional area of radiator tube, square feet

x distance along radiator tube, feet

y distance from axis of radiator tube, feet

T absolute temperature, $^{\circ}F + 460$

T_w absolute temperature of inner surface of radiator tube, $^{\circ}F + 460$

T_s absolute stagnation temperature, $^{\circ}F + 460$, $\left(T + \frac{V^2}{2Jc_p}\right)$

$\theta = T_w - T_s$

ρ density of cooling air, slugs per cubic foot

R_G gas constant for air (53.3 × 32.2 Btu per slug per $^{\circ}F$)

p absolute static pressure, pounds per square foot

q dynamic pressure, pounds per square foot

q_c impact pressure, pounds per square foot

H total pressure, pounds per square foot

Δp_F static-pressure change due to shearing force at tube wall, pounds per square foot

Δp_m static-pressure change due to momentum change of cooling air, pounds per square foot

γ isentropic-expansion exponent (1.4)

k thermal conductivity, Btu per square foot per second per ($^{\circ}$F/foot)

c_p specific heat of air at constant pressure (7.73 Btu per slug per $^{\circ}$F)

J mechanical equivalent of heat (778 foot-pounds per Btu)

h heat-transfer coefficient, Btu per second per square foot per $^{\circ}$F

Q heat-transfer rate, Btu per second

P_c heat-transfer rate, horsepower per unit frontal area of radiator

P_D drag power, horsepower per unit frontal area of radiator

σ relative density of atmosphere ($\rho/0.002378$)

μ absolute viscosity of cooling air, slugs per foot per second

R Reynolds number of flow in radiator tube ($V_2\rho_2 D/\mu$)

a speed of sound at temperature T, feet per second $\left(\sqrt{\gamma R_G T}\right)$

Subscripts:

o in free stream

2 just inside radiator-tube entrance

3 just inside radiator-tube exit

4 just outside radiator-tube exit after sudden expansion

5 in cooling air after air returns to free-stream static pressure

s stagnation

ANALYSIS OF THE COOLING-AIR FLOW

The path of the cooling air through the airplane is conveniently considered in four parts. Between the free stream and the inlet to the radiator tubes the air undergoes a change, usually an increase, in static pressure and some loss of total pressure. In flowing through the hot tube the air undergoes a temperature rise and a total-pressure drop. In passing out of the radiator tubes the air suffers a further loss of total pressure. Finally, as the air passes out of the duct into the free stream, the static pressure returns to free-stream static pressure at substantially constant total pressure. A detailed analysis of the processes occurring in these steps follows.

Adiabatic Compression

The temperature at the radiator-tube entrance is given by a statement of the law of the conservation of energy for the adiabatic flow of a perfect gas

$$T_2 = T_o + \frac{1}{2Jc_p}\left(V_o^2 - V_2^2\right) \tag{1}$$

where $\frac{1}{2Jc_p} = 0.832 \times 10^{-4}$ slug per $^{\circ}F$ per foot-pound

The pressure just inside the radiator-tube entrance, unlike the temperature, is not uniquely determined by the airplane speed and the tube-entrance velocity. If the flow from the free stream

up to this point were isentropic, the pressure p_2 would be given by

$$\left(\frac{p_o}{p_2}\right)^{\frac{\gamma-1}{\gamma}} = \frac{\gamma - 1}{2}\left[1 - \left(\frac{V_o}{V_2}\right)^2\right]\frac{V_2^2}{a_2^2} + 1 \qquad (2)$$

The full isentropic pressure rise is generally not developed because of skin friction and flow separation. An estimate of the pressure loss must be made for purposes of calculation.

Heat Transfer

The usual equation for the heat transfer from a radiator tube is derived by equating the heat lost from an elementary length of tube wall to the heat gained by the fluid in flowing through the element. The heat lost is

$$dQ = h(T_w - T)\pi D\, dx \qquad (3)$$

where T is the temperature at any distance x along the radiator tube. The expression for the heat-transfer coefficient from reference 2, with the value of the constant from reference 3, is

$$h = 0.0247 c_p \left(\frac{\mu}{D}\right)^{0.2} (\rho\bar{V})^{0.8} \qquad (4)$$

The heat gained is given by

$$dQ = \frac{\pi D^2}{4}\rho\bar{V}c_p\, dT \qquad (5)$$

If any change in the kinetic energy within the element is neglected, an equation relating T and x may be obtained by eliminating h and dQ among equations (3), (4), and (5). If the variation in the fifth root of the viscosity is neglected,

the equation may be integrated for the initial conditions $T = T_2$ when $x = 0$; thus

$$T_w - T = (T_w - T_2)e^{-4(0.0247)R^{-0.2}\frac{x}{D}} \tag{6}$$

The quantity of heat transferred per unit time up to point x is

$$Q = \rho V \frac{\pi D^2}{4} c_p (T - T_2) \tag{7}$$

Combining equations (6) and (7) results in the usual equation for the heat transfer of radiators

$$Q = \rho V \frac{\pi D^2}{4} c_p (T_w - T_2)\left[1 - e^{-4(0.0247)R^{-0.2}\frac{x}{D}}\right] \tag{8}$$

The empirical formula for the heat-transfer coefficient given by equation (4) is based on tests at low airspeeds for which the heat developed in the laminar sublayer by viscous shearing forces is small when compared with the total heat transfer. Because the heat generated by viscous shearing forces is quadratically dependent on the cooling-air velocity, this heat becomes appreciable at high airspeeds. For such cases Crocco gives the following rule in reference 4: "The transference of heat between any object and a fluid flowing by it, when it is no longer possible to disregard the heat developed by friction, is governed by the same law that applied when it is negligible, provided the temperature to which the fluid is brought by adiabatic arrest is considered as its temperature." In equation (3), that is, the actual temperature should be replaced by the stagnation temperature

$$dQ = h(T_w - T_s)\pi D\, dx \tag{9}$$

The plausibility of equation (9), at least for the limiting case of zero heat transfer, may be shown as follows: Consider the flow in the boundary layer to be essentially two-dimensional,

inasmuch as the radius of curvature of the tube is large compared with the thickness of the boundary layer. Velocity and temperature gradients in the flow direction may be neglected. The change in the total energy of the fluid flowing through an elementary volume is the net heat conducted into the volume by the temperature gradient perpendicular to the flow direction plus the work done on the volume by the viscous shearing forces resulting from the velocity gradient perpendicular to the flow direction. In the form of an equation, the energy balance becomes

$$\rho V \frac{\partial(c_p T_s)}{\partial x} = \frac{\partial}{\partial y}\left(k\frac{\partial T}{\partial y} + \mu \frac{V}{J}\frac{\partial V}{\partial y}\right) \tag{10}$$

If c_p, k, and μ are assumed to be independent of the temperature, equation (10) may be rewritten as

$$\rho V c_p \frac{\partial T_s}{\partial x} = \frac{\partial^2}{\partial y^2}\left(kT + \frac{\mu}{J}\frac{V^2}{2}\right) \tag{11}$$

For the case $\mu c_p/k = 1$, a particular solution of equation (11) is

$$T + \frac{V^2}{2Jc_p} = T_s = \text{Constant} \tag{12}$$

The net heat conducted into the elementary volume is, for this solution, equal to the work done by the volume against viscous shearing forces, so that the total-energy distribution is uniform throughout the boundary layer. It is apparent that at the wall, where $V = 0$ and $T = T_s$, $\frac{\partial T}{\partial y} = 0$; that is, the wall is at temperature T_s and the heat transfer is zero.

The validity of the assumption $\frac{\mu c_p}{k} = 1$ depends upon whether the boundary layer is laminar or turbulent. There will usually be an outer turbulent boundary layer adjoining a laminar sublayer, part of the temperature rise occurring within each. For the laminar sublayer $\frac{\mu c_p}{k} = 0.75$. For the turbulent part of

the boundary layer, however, $\frac{\mu c_p}{k} = 1$ because the effective values of k and μ are greater for turbulent flow than for laminar flow (reference 4). The over-all effects of the variation of $\frac{\mu c_p}{k}$ with the nature of the flow and of the variation of μ, c_p, and k with temperature on the equilibrium temperature of the pipe wall as given by equation (11) are not very great. Frössel in reference 5 observed that air accelerating from rest at atmospheric temperature to supersonic velocities did not appreciably change the tube-wall temperature from atmospheric temperature, even though the temperature of the air dropped more than 100° F.

In the development of the heat-transfer equation for high airspeeds, the kinetic-energy correction must be added to equation (5) before this equation may be used in the high-velocity range; thus

$$dQ = \frac{\pi D^2}{4} \rho \bar{V} \left[c_p \, dT + d\left(\frac{\bar{V}^2}{2J}\right) \right]$$

or

$$dQ = \frac{\pi D^2}{4} \rho \bar{V} c_p \, dT_s \tag{13}$$

If the heat-transfer coefficient is assumed to be the same at high speeds as at low speeds, the solution of equations (13) and (9) is analogous to equation (8):

$$Q = \rho \bar{V} \frac{\pi D^2}{4} c_p \left(T_w - T_{s_2}\right) \left[1 - e^{-4(0.0247) R^{-0.2} \frac{x}{D}} \right] \tag{14}$$

Equation (14) is recommended as a first approximation to the heat-transfer rate at high airspeeds for which experimental data are lacking. The assumption in the derivation that the heat-transfer coefficient remains the same at high speeds as at low speeds is implied in the rule given by Crocco in reference 4. It is an experimental fact (reference 5) that the skin-friction coefficient is independent of the Mach number; and, because the

mechanism causing heat transfer is essentially the same as the mechanism causing skin friction, it seems justifiable to assume in the absence of direct experimental data that the heat-transfer coefficient is also independent of the Mach number.

Static-Pressure Losses in the Tubes

Linear axial-velocity distributions. - The primary cause of static-pressure drop in the flow through a hot radiator tube is the shearing force at the tube wall due to the skin friction. According to reference 3, the static-pressure drop due to skin friction is

$$\Delta p_F = 0.098\rho\bar{V}^2 R^{-0.2}\frac{x}{D}$$

or, in the differential form with due regard for sign,

$$-dp_F = 0.098\rho\bar{V}^2 \frac{R^{-0.2}}{D}\,dx \tag{15}$$

Because the product $\rho\bar{V}$ must be a constant within the tube, the density reduction within the tube results in an acceleration that causes the further pressure drop

$$\Delta p_m = \frac{d}{dx}\left[\int_0^{D/2} \frac{\rho V^2}{\pi D^2/4}\,(2\pi y)\,dy\right]\Delta x$$

When the variable y is changed to $\frac{y}{D/2}$, the expression rewritten in the differential form is

$$-dp_m = \frac{d}{dx}\left[\rho\bar{V}^2\int_0^1 2\left(\frac{V}{\bar{V}}\right)^2 \frac{y}{D/2}\,d\left(\frac{y}{D/2}\right)\right]dx \tag{16}$$

For the Blasius $\frac{1}{7}$-power-law velocity distribution the value of the integral is 50/49. A value of 1 will be assumed; that is, the average velocity is supposed equal to the root-mean-square velocity. In the rest of the paper the bar has been omitted from V and no distinction is indicated between velocity, average velocity, and root-mean-square velocity.

The equation for the total loss of static pressure is given by the sum of equations (15) and (16) as follows:

$$-dp = 0.098\rho V^2 \frac{R^{-0.2}}{D} dx + d\left(\rho V^2\right) \tag{17}$$

As ρV is constant,

$$p_2 - p_3 = 0.098\rho V \frac{R^{-0.2}}{D} \int_0^L V \, dx + \rho V \int_{V_2}^{V_2} dV \tag{18}$$

The static-pressure drop in the tube may be approximated if the axial-velocity distribution is assumed to be linear, an assumption that will be justified in the following section. By this assumption

$$p_2 - p_3 = 0.098\rho_2 V_2 R^{-0.2} \left(\frac{V_2 + V_3}{2}\right) \frac{L}{D} + \rho_2 V_2 \left(V_3 - V_2\right) \tag{19}$$

By use of

$$\rho_2 V_2 = \rho_3 V_3$$

and

$$\frac{p_2}{\rho_2 T_2} = \frac{p_3}{\rho_3 T_3}$$

equation (19) may be solved for $p_2 - p_3$ in terms of the known quantities p_2, ρ_2, V_2, T_3, and L/D:

$$p_2 - p_3 = \frac{1}{2}\left(B - \sqrt{B^2 - 4C}\right) \tag{20}$$

where

$$B = p_2 - \rho_2 V_2^2\left(1 - \frac{F}{2}\right)$$

$$C = p_2 \rho_2 V_2^2\left[\frac{T_3}{T_2}\left(1 + \frac{F}{2}\right) + \left(\frac{F}{2} - 1\right)\right]$$

and

$$F = 2\left(0.049 \frac{L}{D} R^{-0.2}\right)$$

The value of T_3 is obtained from equation (6).

Nonlinear axial-velocity distributions. - When static-pressure drops exceed 30 percent of the absolute pressure at the tube entrance, an error of more than 10 percent will be made in determining the pressure drop from equation (20). In this case the simplified solution of the differential equation for the pressure drop based on the linear axial-velocity distribution is no longer valid. A more precise solution of equation (17) may be derived as follows: First, the axial velocity is expanded as a power series of the x/D ratio with coefficients to be determined. This expression is substituted in equation (17) and the equation is integrated for the pressure as a function of the x/D ratio. By the use of the series development for the stagnation temperature, the coefficients of the power series are finally determined.

Expanding the axial velocity in terms of the x/D ratio gives

$$V = V_2 + a\left(\frac{x}{D}\right) + b\left(\frac{x}{D}\right)^2 + c\left(\frac{x}{D}\right)^3 + d\left(\frac{x}{D}\right)^4 \ldots \tag{21}$$

which is substituted in equation (17) rewritten as

$$-dp = \rho V \left[mV + \frac{dV}{d\left(\frac{x}{D}\right)} \right] d\left(\frac{x}{D}\right)$$

where $m = 0.098R^{-0.2}$. There is thus obtained for the axial-pressure distribution

$$p = p_2 - \rho V m \left[V_2\left(\frac{x}{D}\right) + \frac{a}{2}\left(\frac{x}{D}\right)^2 + \frac{b}{3}\left(\frac{x}{D}\right)^3 + \frac{c}{4}\left(\frac{x}{D}\right)^4 \cdots \right]$$

$$- \rho V \left[a\left(\frac{x}{D}\right) + b\left(\frac{x}{D}\right)^2 + c\left(\frac{x}{D}\right)^3 + d\left(\frac{x}{D}\right)^4 \cdots \right] \qquad (22)$$

If T is replaced by T_s and θ is defined as $T_w - T_s$, there is obtained from equation (6):

$$\theta = \theta_2 e^{-m\left(\frac{x}{D}\right)} = \theta_2 \left[1 - m\left(\frac{x}{D}\right) + \frac{m^2\left(\frac{x}{D}\right)^2}{2!} - \frac{m^3\left(\frac{x}{D}\right)^3}{3!} \cdots \right] \qquad (23)$$

From the definition of T_s

$$T_w - T_s = T_w - T + \frac{V^2}{2Jc_p}$$

and the gas law

$$p = \rho R_G T$$

θ may be written as

$$\theta = T_w - \frac{pV}{R_G \rho V} - \frac{V^2}{2Jc_p} \qquad (24)$$

Linear equations for the coefficients in the power series of equation (21) are obtained by substituting the expressions for V, p, and θ given by equations (21), (22), and (23), respectively, in equation (24) and setting the sum of the coefficients of the various powers of the $\frac{x}{D}$ ratio equal to zero:

$$\left.\begin{aligned}
\beta a &= m\left(\frac{V_2^2}{R_G} + \theta_2\right) \\
\beta b &= \frac{3mV_2a}{2R_G} + \frac{a^2(\gamma + 1)}{2\gamma R_G} - \frac{\theta_2 m^2}{2!} \\
\beta c &= \frac{m}{R_G}\left(\frac{4V_2b}{3} + \frac{a^2}{2}\right) + \frac{ab(\gamma + 1)}{\gamma R_G} + \frac{\theta_2 m^3}{3!} \\
\beta d &= \frac{5m}{R_G}\left(\frac{V_2c}{4} + \frac{ab}{6}\right) + \frac{\gamma + 1}{2\gamma R_G}(2ac + b^2) - \frac{\theta_2 m^4}{4!} \\
\beta e &= \frac{3m}{R_G}\left(\frac{2V_2d}{5} + \frac{ac}{4}\right) + \frac{\gamma + 1}{\gamma R_G}(ad + bc) + \frac{mb^2}{3R_G} + \frac{\theta_2 m^5}{5!}
\end{aligned}\right\} \quad (25)$$

where

$$\beta = \frac{T_w - \theta_2}{V_2} - \frac{V_2}{\gamma R_G}$$

The coefficients a, b, c, d, and e are thus determined in terms of T_w and the entrance conditions m, V_2, and θ_2. The pressure drop for any value of x/D is found by substituting these values in equation (22) or in the following rearrangement of equation (22):

$$p_2 - p = \rho V\left[\left(mV_2 + a\right)\frac{x}{D} + \left(\frac{ma + 2b}{2}\right)\left(\frac{x}{D}\right)^2 + \left(\frac{mb + 3c}{3}\right)\left(\frac{x}{D}\right)^3 + \left(\frac{mc + 4d}{4}\right)\left(\frac{x}{D}\right)^4 \cdots\right] \quad (26)$$

The rapidity of convergence of the right-hand side of equation (26) has been investigated by a graphical integration of equation (17) for specific initial conditions. In figure 1 the results of this integration are compared with the results obtained by use of equation (26). Mathematical accuracy compatible with the other simplifying assumptions of this analysis is obtained for pressure ratios down to 0.55 by using five terms of the power series.

Figure 1 is also useful for checking the accuracy of equation (20), which was derived by assuming a linear axial-velocity distribution. Equation (20) appears to be reasonably accurate throughout the present design range and down to a pressure ratio p_3/p_2 of 0.7.

Another approximate solution for equation (17), based on the use of the stagnation temperature in the gas law, is

$$\log_e \frac{p_2}{p_3}\left(\frac{T_w - T_{s_2}}{T_w - T_{s_3}}\right)\left(\frac{T_{s_3}}{T_{s_2}}\right) = \frac{p_2^2\left[1 - \left(\frac{p_3}{p_2}\right)^2\right]}{(\rho V)^2 R_G\left(T_{s_3} + T_{s_2}\right)} \tag{27}$$

where

$$T_{s_3} = T_{s_2} + \theta_2\left[1 - e^{-m\left(\frac{x}{D}\right)}\right]$$

The accuracy of this solution, as indicated in figure 1 is between the accuracies of the two solutions already discussed.

Effect of Mach number on flow in radiator tubes. - Important information concerning the effect of Mach number on flow in radiator tubes can be obtained from equation (17). From equation (23)

$$\theta = \theta_2 e^{-0.098R^{-0.2}\frac{x}{D}}$$

which, when differentiated, is

$$\frac{d\theta}{\theta} = -0.098\,\frac{R^{-0.2}}{D}\,dx \tag{28}$$

Substituting directly in equation (17) results in

$$-dp = (-\rho V)V \frac{d\theta}{\theta} + \rho V \, dV \tag{29}$$

If dp is now eliminated from equation (29) by means of the two relationships

$$p = \rho R_G T$$

and

$$T + \frac{V^2}{2Jc_p} = T_s$$

the resulting equation in two variables is

$$\frac{d\theta}{dV} = \frac{\theta}{V} \frac{V^2\left(1 - \frac{R_G}{2Jc_p}\right) + R_G\left(\theta - T_w\right)}{R_G\theta + V^2} \tag{30}$$

Equation (30) is important because it is independent of geometry and Reynolds number.

At present no closed solution of equation (30) is available. A graphical solution, determined by the isoclinic method, is given in figure 2. The curve for any particular radiator is the curve that passes through the point $\left(V_2^2, \theta_2\right)$ corresponding to the given entrance conditions. The straight line in the figure separates the supersonic range on the right from the subsonic range on the left. The equation of the straight line is found by setting $d\theta/dV$ equal to zero in equation (30)

$$V^2\left(1 - \frac{R_G}{2Jc_p}\right) = R_G\left(T_w - \theta\right) \tag{31}$$

This equation may be easily reduced, from the definition of θ, to $\frac{V}{a} = 1$; that is, the line corresponds to a Mach number of unity.

If the entrance velocity V_2 is subsonic, V will increase along the tube and may reach sonic velocity, where $\frac{d\theta}{dV} = 0$. For the air to accelerate into the supersonic region, θ would have to increase; that is, the total energy would have to decrease, which is contrary to equation (23), the heat-transfer equation. A supersonic velocity may then never develop within a radiator tube with subsonic entrance velocity. The limiting Mach number of unity will be found at the tube exit.

If the entrance velocity is supersonic, V will decrease along the tube, the change being now from right to left along the curves of figure 2. The flow may not, however, pass continuously into the subsonic region without violating equation (23). A discontinuous transition may occur from the supersonic to the subsonic region by means of a stationary compression shock if the upstream flow is supersonic, depending on the tube length and the exit pressure. Such phenomena, however, are of no importance in current radiator technology and a discussion of them is beyond the scope of this paper.

Pressure loss at the exit of the radiator tubes. - For radiators in current use the discharge of the air from the radiator tubes is accompanied by a loss of total pressure of about $0.2q_3$ (reference 2, p. 10). This loss somewhat exceeds that given by the well-known Borda-Carnot formula for expansion loss

$$\Delta H = q_3 \left(1 - \frac{A_3}{A_4}\right)^2 \tag{32}$$

which, for $\frac{A_3}{A_4} = \frac{2}{3}$, is only $0.11q_3$. The difference is probably due partly to surface irregularities at the exit and partly to the difference in kinetic energies associated with the upstream and the downstream velocity distributions.

Outlet flow. - For convenience in computation, the air behind the radiator is assumed to be brought to stagnation conditions.

The stagnation pressure is then

$$p_{s_4} = p_3\left(1 + \frac{\gamma - 1}{2\gamma}\frac{V_3^2}{R_G T_3}\right)^{\frac{\gamma}{\gamma-1}} = 0.2q_3 \tag{33}$$

and, from equation (6), the stagnation temperature is

$$T_{s_4} = T_{s_2} + \left(T_w - T_{s_2}\right)\left[1 - e^{-4(0.0247)R^{-0.2}\frac{L}{D}}\right] \tag{34}$$

The air is now assumed to expand isentropically to the free-stream pressure. The velocity of the air at this pressure is given by

$$V_5 = \sqrt{2Jc_p\left(T_{s_4} - T_5\right)} = \sqrt{2Jc_p\, T_{s_4}\left(1 - \frac{T_5}{T_{s_4}}\right)} \tag{35}$$

Introducing the relationship

$$\frac{T_{s_4}}{T_5} = \left(\frac{p_{s_4}}{p_o}\right)^{\frac{\gamma-1}{\gamma}} \tag{36}$$

allows equation (35) to be rewritten as

$$V_5 = \sqrt{2Jc_pT_{s_4}\left[1 - \left(\frac{p_o}{p_{s_4}}\right)^{\frac{\gamma-1}{\gamma}}\right]} \tag{37}$$

The drag power per unit open area due to the momentum change of the cooling air is

$$P_D = \frac{\rho_2 V_2 (V_o - V_5) V_o}{550} \qquad (38)$$

It is to be noted that this power represents, in general, a practical minimum as this value neglects any further effects of the low-energy cooling air on the external drag.

PERFORMANCE CHARTS

For the radiator performance charts the pressure drops within the radiator tubes were, for convenience, calculated by the simplest of the methods discussed, namely, the method that assumes a linear velocity distribution along the tube. As has already been indicated, the pressure losses are thereby slightly overestimated for those cases in which the pressure drop is a large fraction of the absolute pressure. The calculation of the flow path of the cooling air to obtain the performance charts is outlined as follows:

Values of airplane speed, altitude, and tube-entrance velocity are assumed. The temperature T_2 at the tube entrance follows from equation (1), but the pressure p_2 given by equation (2) is arbitrarily reduced by 10 percent of the free-stream dynamic pressure to account for flow separation and skin friction. The heat-transfer rate follows from equation (14) by evaluating the viscosity in the Reynolds number at the mean air temperature approximated by use of equation (6). The pressure at the radiator exit follows from equation (20), where T_3 is approximated by equation (6). The stagnation pressure and the temperature in the duct behind the radiator follow from equations (33) and (34), respectively. Finally, the drag power is obtained from equation (38) with the exit velocity of equation (37). The atmospheric conditions were assumed to be those of Army air and the radiator-tube-wall temperature was assumed to be 240° F. A ratio of free-flow area to frontal area of 2/3 was assumed; for any other ratio, the results merely change in proportion.

The calculations covered the following ranges of variables:

Altitude, ft	0 to 50,000
Airspeed, mph	0 to 500
Radiator-tube length, in.	9, 12, and 15
Radiator-tube diameter, in.	1/4 and 1/5

The six performance charts of figure 3 are for the six different radiators. In these charts the total-pressure loss, defined as the difference between the stagnation pressures ahead of and behind the radiator, has been plotted against the heat-transfer rate per unit frontal area. The inlet pressure loss is not included. The ordinates have been divided by σ for NACA standard air (see table I) merely for convenience in separating the curves. Lines of constant tube-entrance velocity have also been plotted in figure 3 to aid in the quick determination of the cooling-air quantity at the radiator face.

Although the calculations were carried out for airplane speeds of 100 miles per hour to 500 miles per hour, the results plotted in figure 3 are only for an airplane speed of 300 miles per hour. The ratio of the heat-transfer rate at several airplane speeds to the heat-transfer rate at an airplane speed of 300 miles per hour for the same total-pressure loss has been tabulated for different altitudes in table II. These corrections, although appreciable in some cases, especially at the lower altitudes, are for the most part negligible. A similar correction for the cooling-air quantity is given in table III, where the ratios of the tube-entrance airspeeds at several airplane speeds to the tube-entrance airspeed at an airplane speed of 300 miles per hour for the same loss in total pressure are tabulated for different altitudes.

It may be remarked that the corrections in table II involve two opposing effects of airplane speed: namely, increased tube-entrance stagnation temperature, which decreases the heat-transfer rate for a given total pressure loss, and increased tube-entrance density, which has the opposite effect. At low altitudes, the temperature effect predominates; but at high altitudes, where the critical design condition usually occurs, these effects almost compensate each other and render figure 3 particularly accurate.

A comparison of figures 3(a) and 3(d) shows that about 50 percent more heat may be dissipated per unit flow area by $\frac{1}{5}$-inch tubes 9 inches long than by $\frac{1}{4}$-inch tubes 9 inches long for the same total-pressure loss. In general, for tube lengths of this order, the tubes of smaller diameter will permit smaller radiators and/or smaller total-pressure losses.

Figure 4 shows the drag characteristics of the radiators as functions of the flight speed, the heat-transfer rate, and the tube-entrance velocity. The heat-transfer rate and the tube-entrance velocity are obtained from figure 3. No interference effects or weight drag are included. It may be seen that, at the high inlet velocities necessary at high altitudes with radiators of reasonable size, the cooling drag power becomes very high.

In the past it was hoped that the Meredith phenomenon would bring about very low drags at high altitudes. Appreciable decreases in drag are due to this source; but the calculations, which automatically take into account the Meredith phenomenon, show that these decreases are not sufficient to keep the drag of small-size high-pressure-drop units from appreciably increasing at high altitudes.

An example will illustrate the use of figures 3 and 4 and of table II. The airplane for which the radiator will be designed is assumed to have the performance shown in table I. The densities and Mach numbers used in calculating q_c are for Army air. The radiator design is assumed to be for tubes of $\frac{1}{4}$-inch internal diameter and 9-inch length.

The usual condition determining the radiator frontal area will be either climb at sea level or climb at the maximum altitude, that is, the condition at which the heat-transfer rate per unit frontal area is lowest when the entire total pressure available for cooling is utilized. If the available pressure for cooling is assumed to be $0.9q_c$, the values of the heat-transfer rate may be read from figure 3(a) for both high speed and climb. The results, corrected according to table II, are summarized in table IV.

An examination of table IV discloses that the frontal area of the radiator is determined by the value of the heat-transfer rate in climb at 40,000 feet, if the necessary heat-transfer rate for satisfactory cooling is assumed constant. If 1000 horsepower is to be transferred to the cooling air, the necessary radiator frontal area is 1000/164 or 6 square feet.

Once the radiator frontal area is fixed, the operating line of the radiator is the ordinate in figure 3 through a heat-transfer

rate of 164 horsepower per square foot. The ratio of the drag power to the heat-transfer rate may be determined from figure 4(a) from the values of the airplane speed, the tube-entrance velocity, and the altitude. The results are tabulated in table V.

CONCLUSIONS

From the present study of heat transfer, pressure drop, and drag power of radiators in flight at high altitudes, it is concluded that:

1. At high altitudes, the density reduction within the radiator tubes results in appreciable increases in both friction pressure drop and acceleration pressure drop.

2. The usual heat-transfer equations may be retained at high Mach numbers, provided that stagnation temperature is used in place of actural temperature.

3. Heat-transfer rate as a function of pressure loss is practically independent of airplane speed at high altitudes.

4. Excessive drag is associated with the use of small radiators at high altitudes; slight increases in radiator size result in large decreases in drag.

5. The Meredith phenomenon becomes insignificant when the radiator pressure drop approaches the total available pressure.

Langley Memorial Aeronautical Laboratory
National Advisory Committee for Aeronautics
Langley Field, Va.

REFERENCES

1. Silverstein, Abe: High-Altitude Cooling. I - Résumé of the Cooling Problem. NACA ARR No. L4I11, 1944.

2. Brevoort, M. J., and Leifer, M.: Radiator Design and Installation. NACA ACR, May 1939.

3. Brevoort, M. J.: Radiator Design. NACA ACR, July 1941.

4. Crocco, Luigi: Transmission of Heat from a Flat Plate to a Fluid Flowing at a High Velocity. NACA TM No. 690, 1932.

5. Frössel, W.: Flow in Smooth Straight Pipes at Velocities above and below Sound Velocity. NACA TM No. 844, 1938.

TABLE I. - ASSUMED AIRPLANE PERFORMANCE

[Wing loading, 40 lb/sq ft; heat rejection, 1000 hp]

Altitude (ft)	Relative density, σ (a)	High speed			Climb		
		Air-speed, V (mph)	Free-stream impact pressure, q_c (lb/sq ft)	$\frac{0.9q_c}{\sigma}$	Air-speed, V (mph)	Free-stream impact pressure, q_c (lb/sq ft)	$\frac{0.9q_c}{\sigma}$
0	1.000	333	275	247	192	87	78.3
10,000	.738	367	247	301	218	84	102.4
20,000	.533	403	220	371	246	77	130.2
30,000	.374	450	190	456	280	70	168.5
40,000	.245	501	170	625	354	79	290.0

[a]The values of σ are based on NACA standard air as in fig. 3.

TABLE II. - RATIO OF HEAT-TRANSFER RATES AT SEVERAL AIRPLANE SPEEDS TO HEAT-TRANSFER RATE AT AN AIRPLANE SPEED OF 300 MILES PER HOUR FOR IDENTICAL TOTAL-PRESSURE LOSSES, $\frac{P_c}{(P_c)_{300}}$

	$P_c/(P_c)_{300}$					
V_o (mph) \ Altitude (ft)	0	10,000	20,000	30,000	40,000	50,000
100	1.08	1.05	1.03	1.02	1.00	1.00
200	1.05	1.03	1.02	1.01	1.00	1.00
300	1.00	1.00	1.00	1.00	1.00	1.00
400	.93	.95	.97	.98	.99	1.00
500	.83	.88	.92	.95	.98	.99

TABLE III. - RATIO OF TUBE-ENTRANCE AIRSPEEDS AT SEVERAL AIRPLANE SPEEDS TO TUBE-ENTRANCE AIRSPEED AT AN AIRPLANE SPEED OF 300 MILES PER HOUR FOR IDENTICAL TOTAL-PRESSURE LOSSES, $\frac{V_2}{(V_2)_{300}}$

	$V_2/(V_2)_{300}$					
V_o (mph) \ Altitude (ft)	0	10,000	20,000	30,000	40,000	50,000
100	1.05	1.05	1.05	1.06	1.06	1.06
200	1.03	1.03	1.03	1.03	1.04	1.04
300	1.00	1.00	1.00	1.00	1.00	1.00
400	.96	.96	.96	.95	.95	.95
500	.92	.91	.91	.90	.89	.89

TABLE IV. - VARIATION WITH ALTITUDE OF MAXIMUM POSSIBLE COOLING PER SQUARE FOOT

Altitude (ft)	High speed				Climb			
	Airspeed (from table I) (mph)	$(P_c)_{300}$ (from fig. 3(a)) (hp / sq ft)	$\frac{P_c}{(P_c)_{300}}$ (from table II)	P_c (hp / sq ft)	Airspeed (mph)	$(P_c)_{300}$ (hp / sq ft)	$\frac{P_c}{(P_c)_{300}}$ (from table II)	P_c (hp / sq ft)
0	333	305	0.98	299	192	190	1.05	199
10,000	367	300	.97	291	218	200	1.03	206
20,000	403	282	.97	274	246	193	1.01	195
30,000	450	235	.97	228	280	175	1.00	175
40,000	501	195	.98	191	354	164	1.00	164

NATIONAL ADVISORY
COMMITTEE FOR AERONAUTICS

TABLE V. - PERFORMANCE OF RADIATOR OF 6-SQUARE-FOOT FRONTAL AREA TRANSFERRING 1000 HORSEPOWER

Altitude (ft)	V_2 (from fig. 3(a)) (mph)	High speed			Climb		
		V_o (from table I) (mph)	P_D/P_c (from fig. 4(a))	P_D (hp)	V_o (mph)	P_D/P_c	P_D (hp)
0	130	333	0.102	102	192	0.124	124
10,000	135	367	.072	72	218	.108	108
20,000	145	403	.064	64	246	.102	102
30,000	172	450	.104	104	280	.200	200
40,000	220	501	.176	176	354	.360	360

L-773

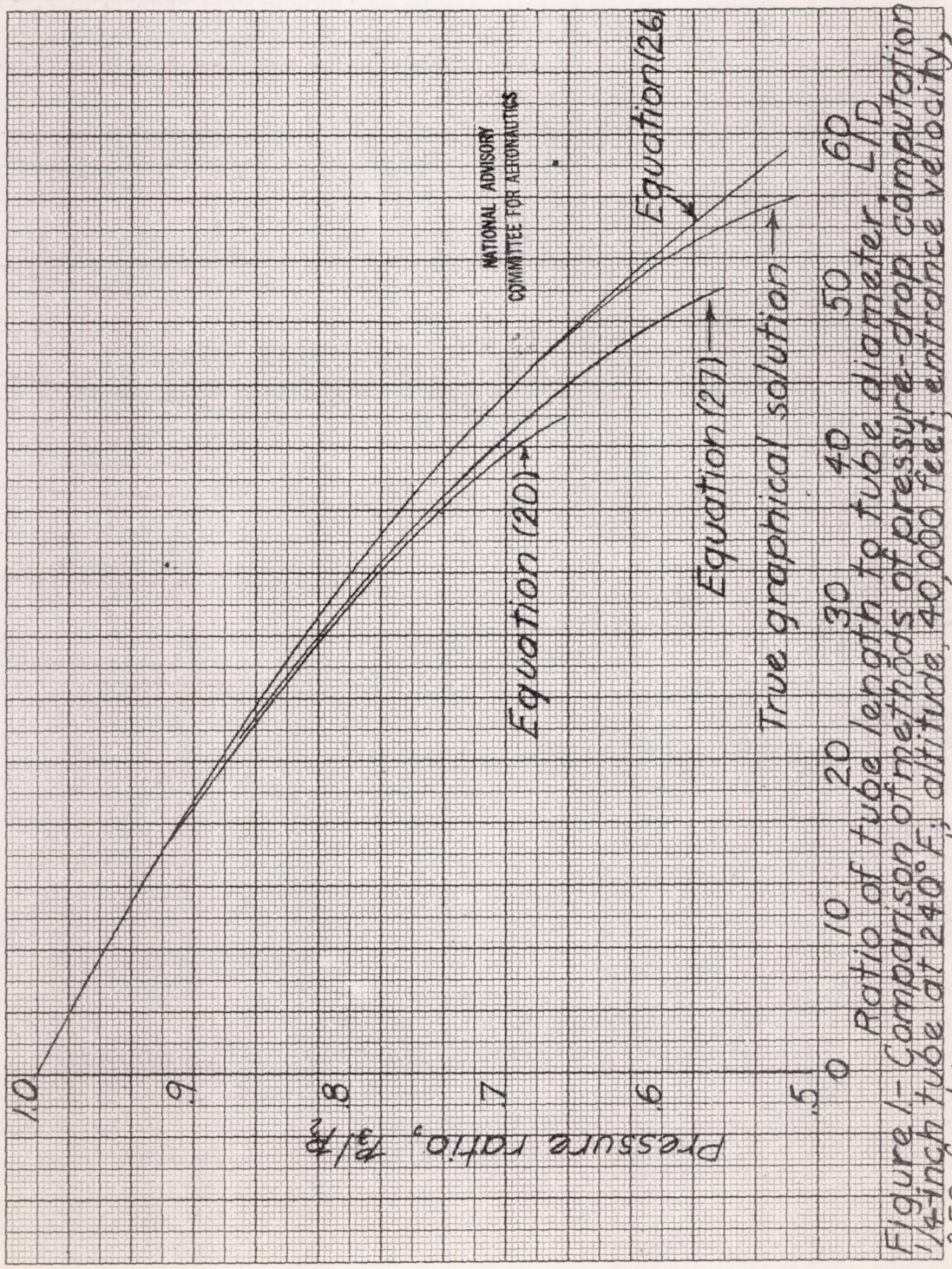

Figure 1.- Comparison of methods of pressure-drop computation; 1/4-inch tube at 240° F, altitude, 40,000 feet, entrance velocity, 350 feet per second.

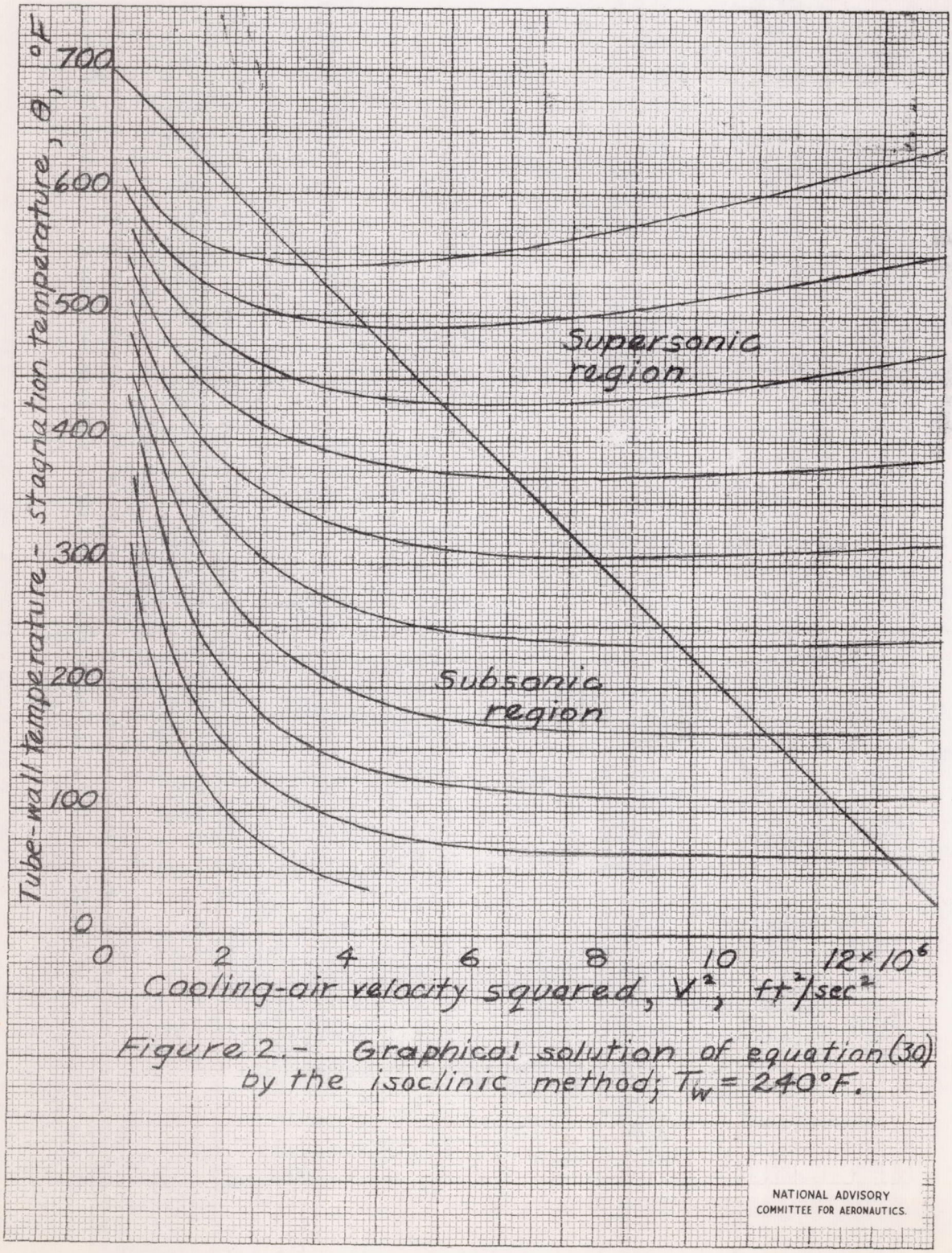

Figure 2.- Graphical solution of equation (30) by the isoclinic method; $T_w = 240°F$.

L-773

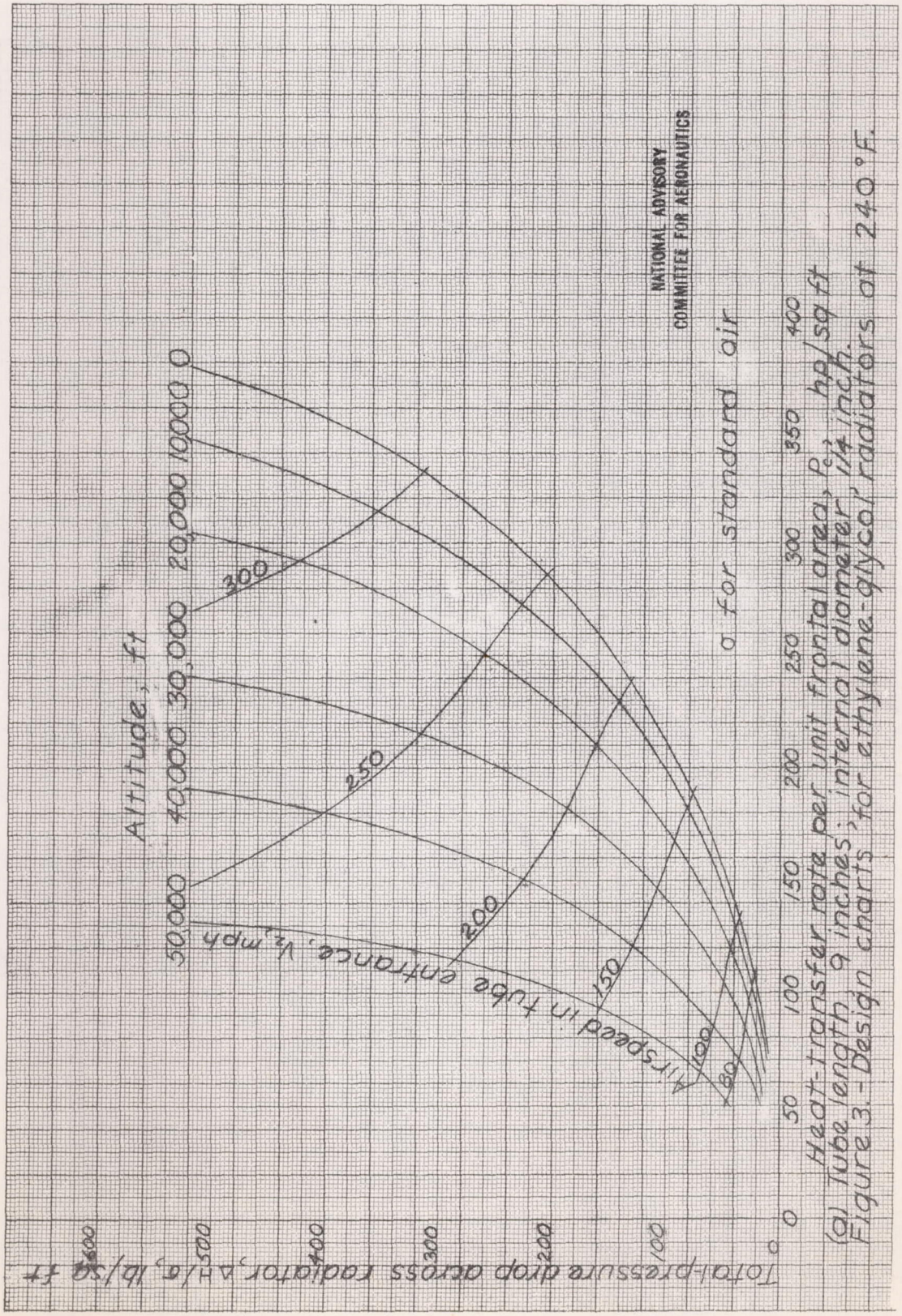
NATIONAL ADVISORY
COMMITTEE FOR AERONAUTICS
Total-pressure drop across radiator, $\Delta H/\sigma$, lb/sq ft
Altitude, ft
Air speed in tube entrance, V_2, mph
Heat-transfer rate per unit frontal area, P_e, hp/sq ft
0 for standard air
(a) Tube length, 9 inches; internal diameter, 1/4 inch.
Figure 3.- Design charts for ethylene-glycol radiators at 240°F.

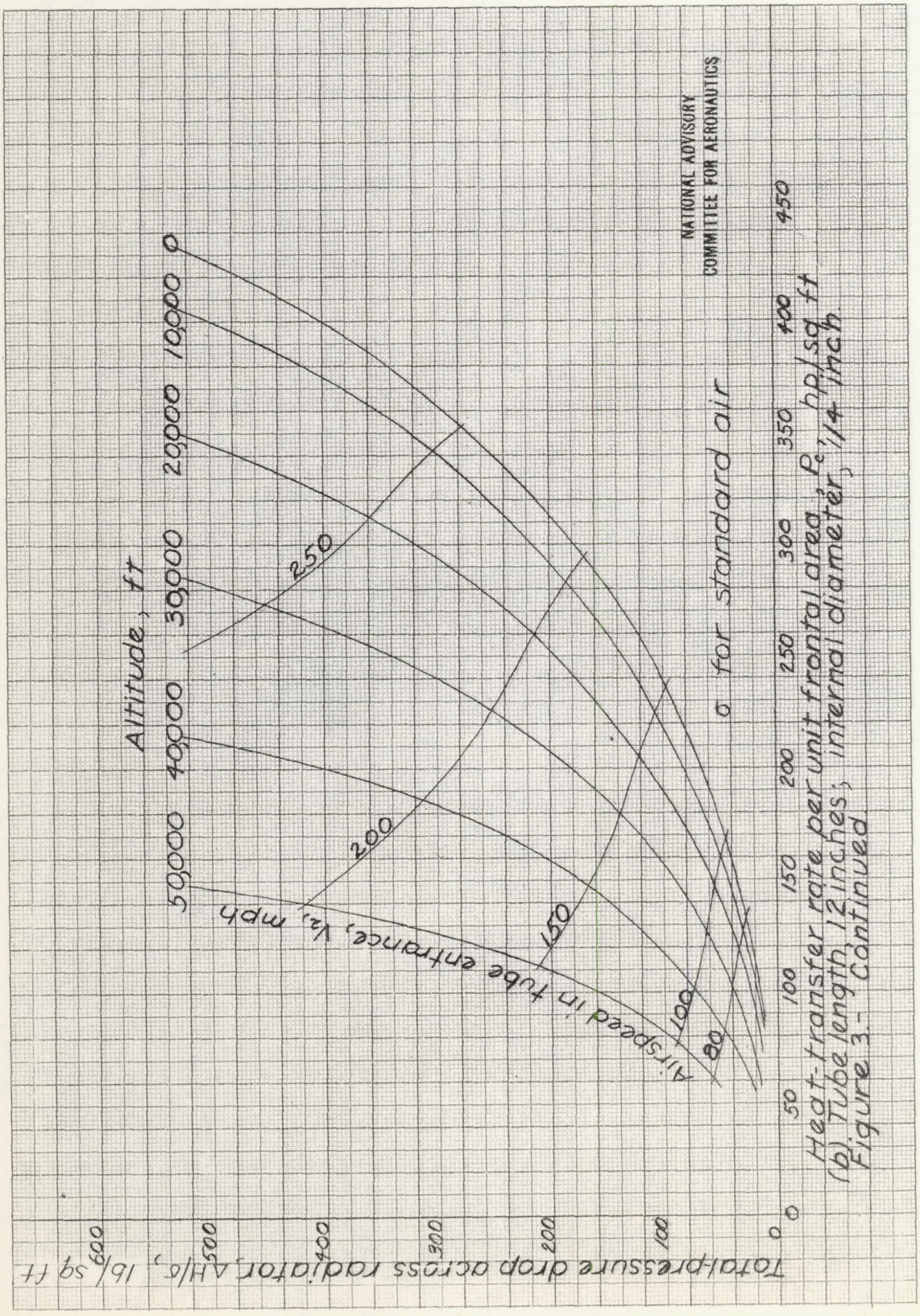

(b) Tube length, 12 inches; internal diameter, 1/4 inch.

Figure 3.- Continued.

L-773.

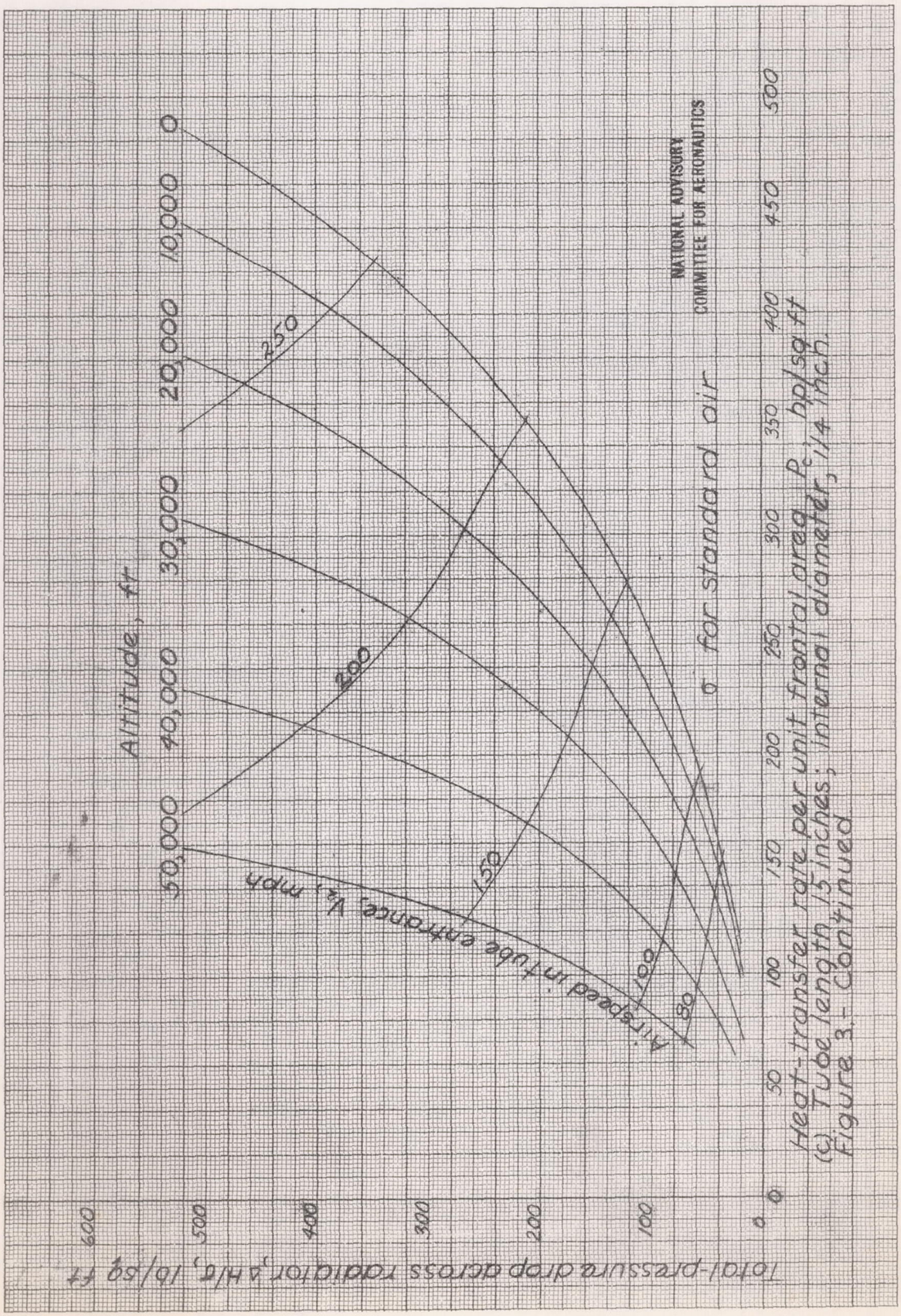
Heat-transfer rate per unit frontal area, P_c, btu/sq ft
(c) Tube length, 15 inches; internal diameter, 1/4 inch
Figure 3.- Continued
σ for standard air
NATIONAL ADVISORY COMMITTEE FOR AERONAUTICS
Altitude, ft
Airspeed in tube entrance, V_t, mph
Total-pressure drop across radiator, ΔH_t, lb/sq ft

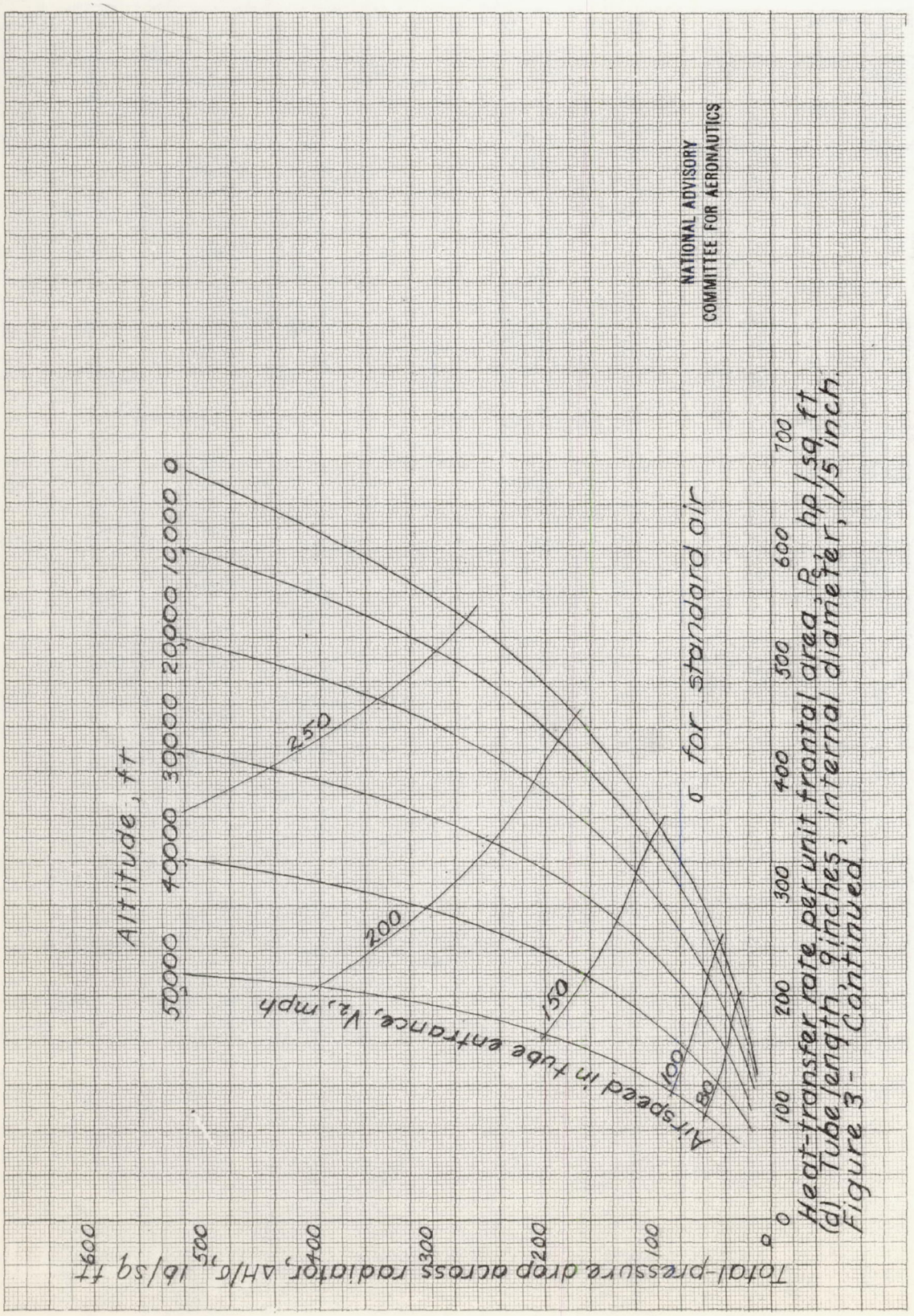

(d) Tube length, 9 inches; internal diameter, 1/5 inch.
Figure 3- Continued

L-773

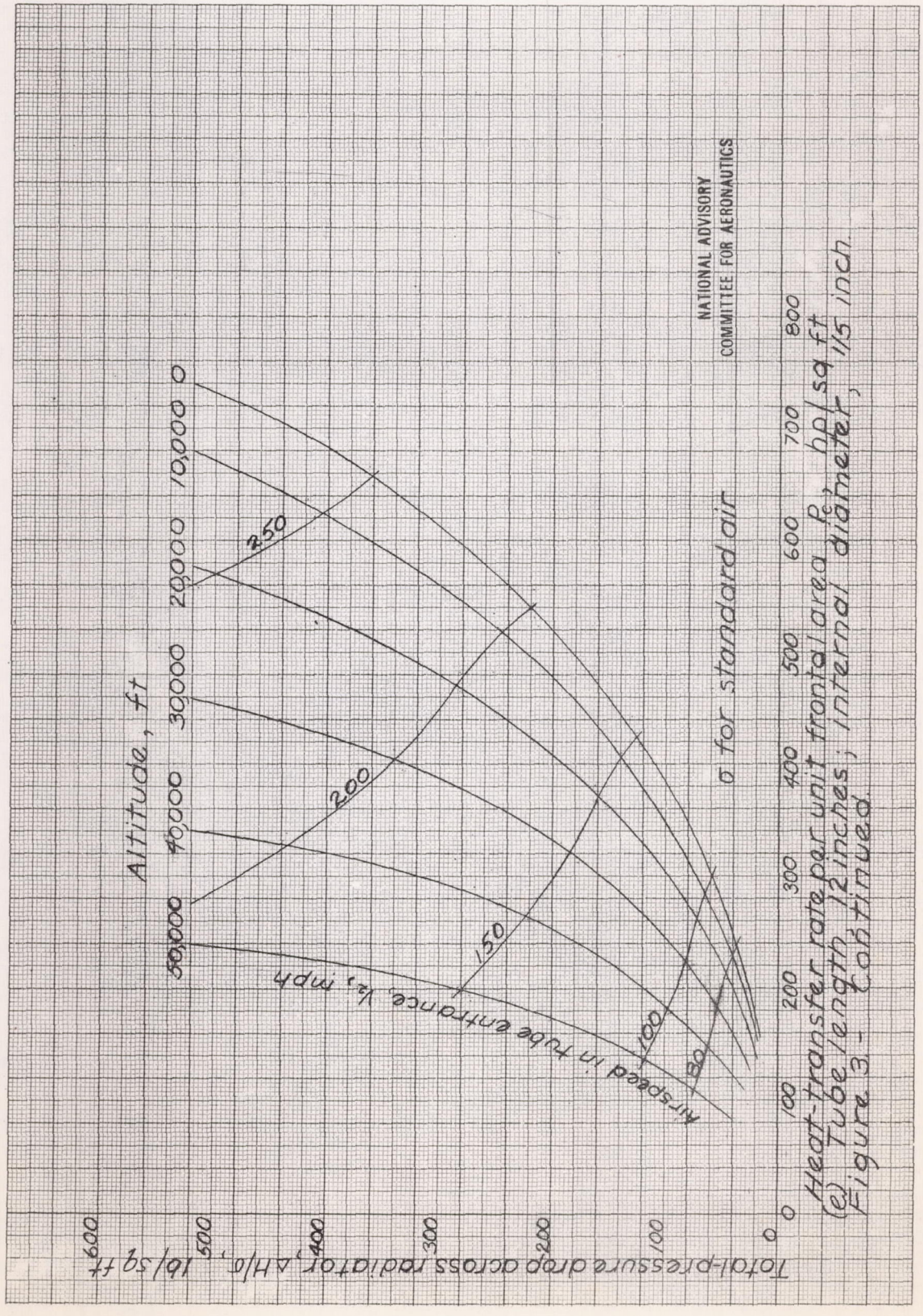

(e) Heat-transfer rate per unit frontal area R_e, 60 lb/sq ft
Tube length, 12 inches; internal diameter, 1/5 inch
Figure 3 - Continued.

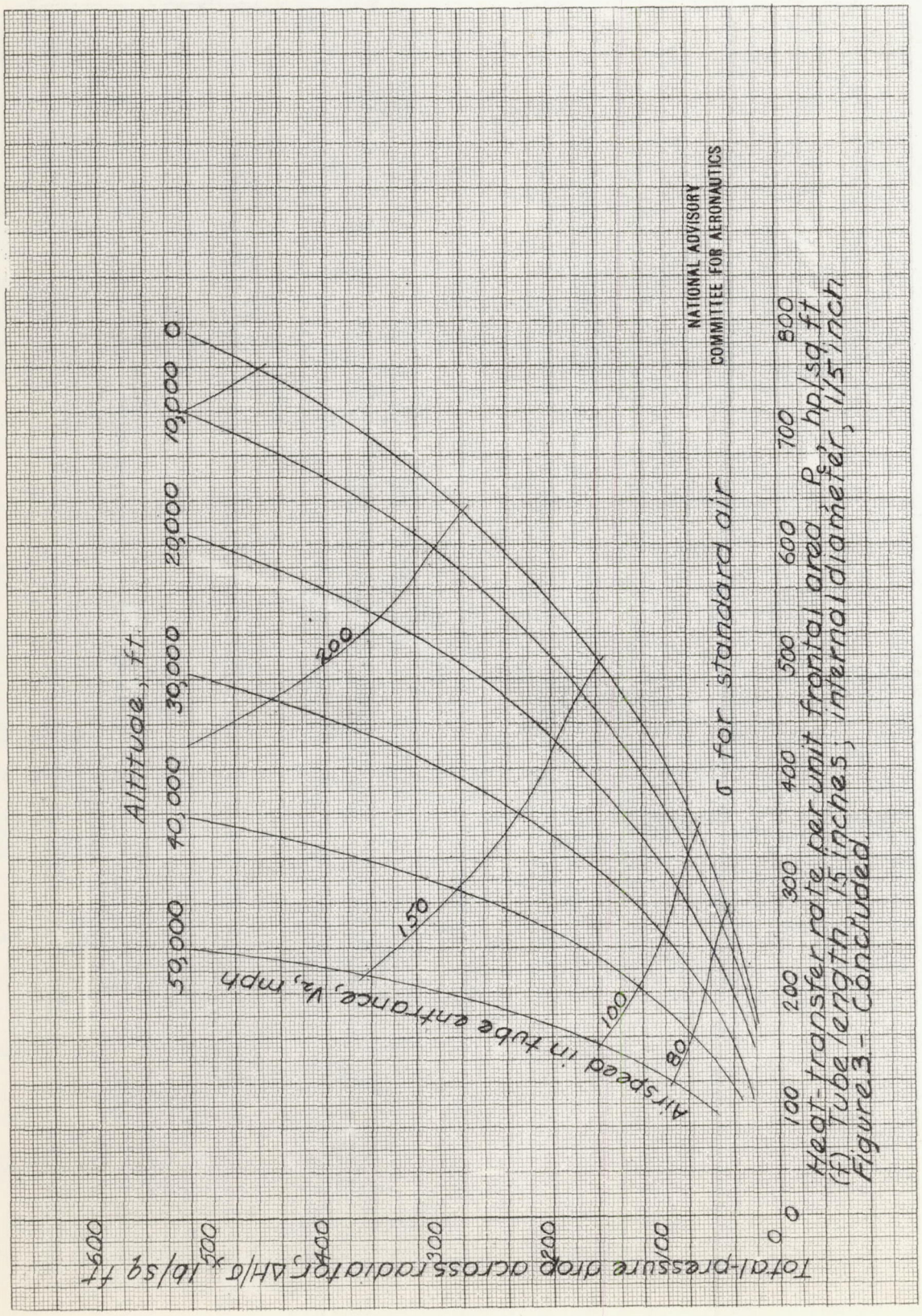

(f) Tube length, 15 inches; internal diameter, 1/5 inch.

Figure 3 - Concluded.

L-773

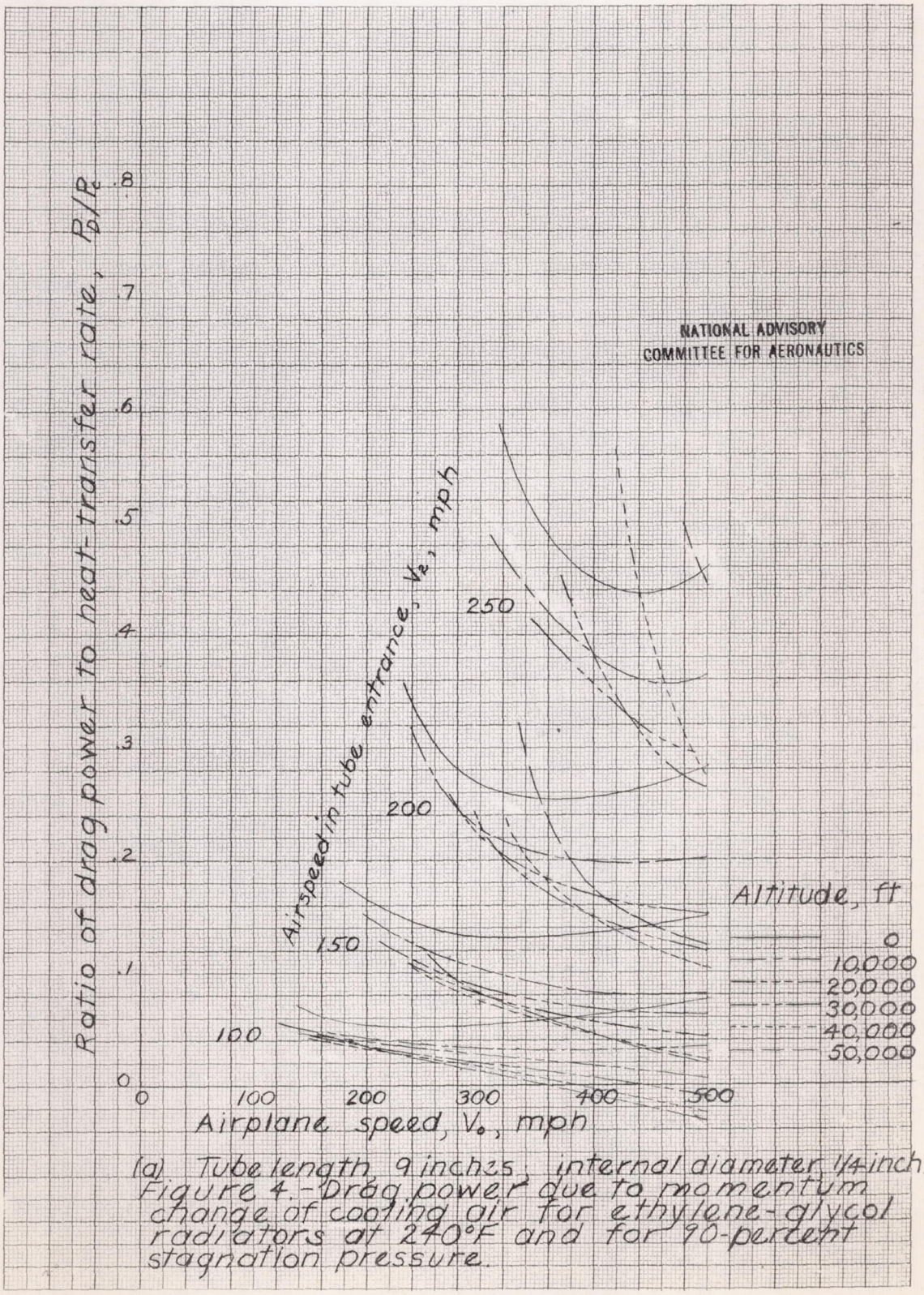

(a) Tube length, 9 inches; internal diameter, 1/4 inch.

Figure 4.- Drag power due to momentum change of cooling air for ethylene-glycol radiators at 240°F and for 90-percent stagnation pressure.

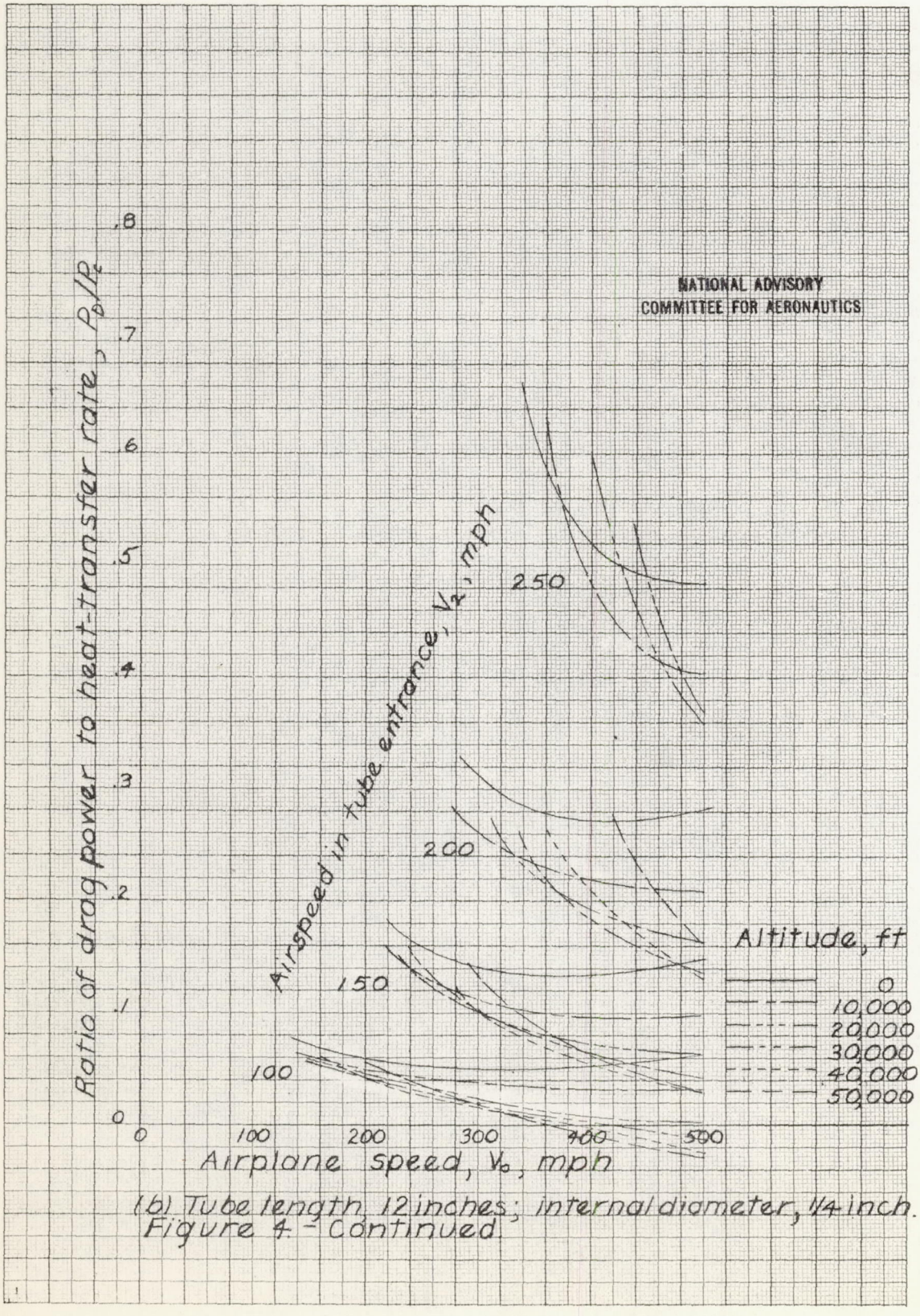

(b) Tube length, 12 inches; internal diameter, 1/4 inch.

Figure 4 - Continued.

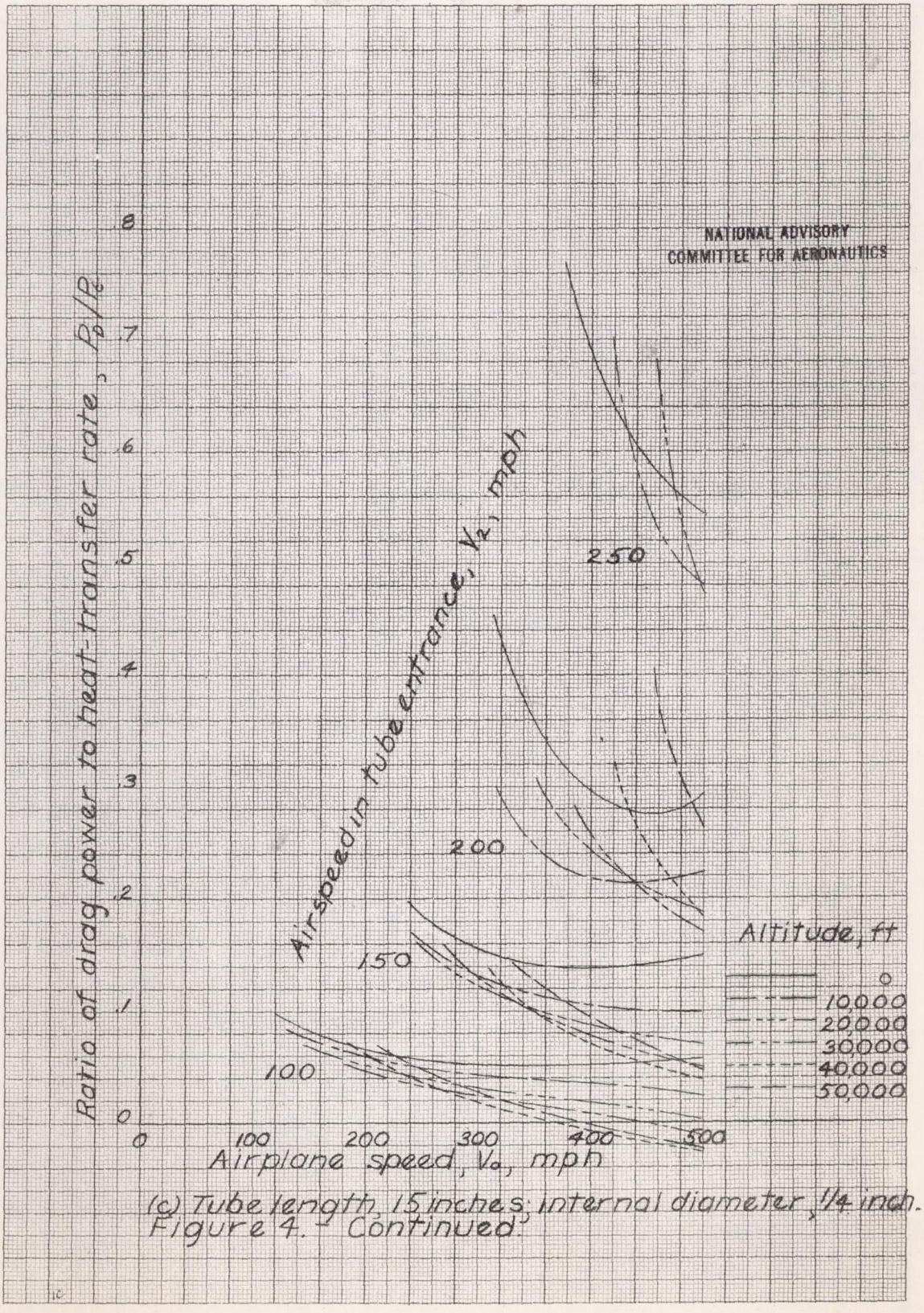

(c) Tube length, 15 inches; internal diameter, 1/4 inch.

Figure 4.- Continued.

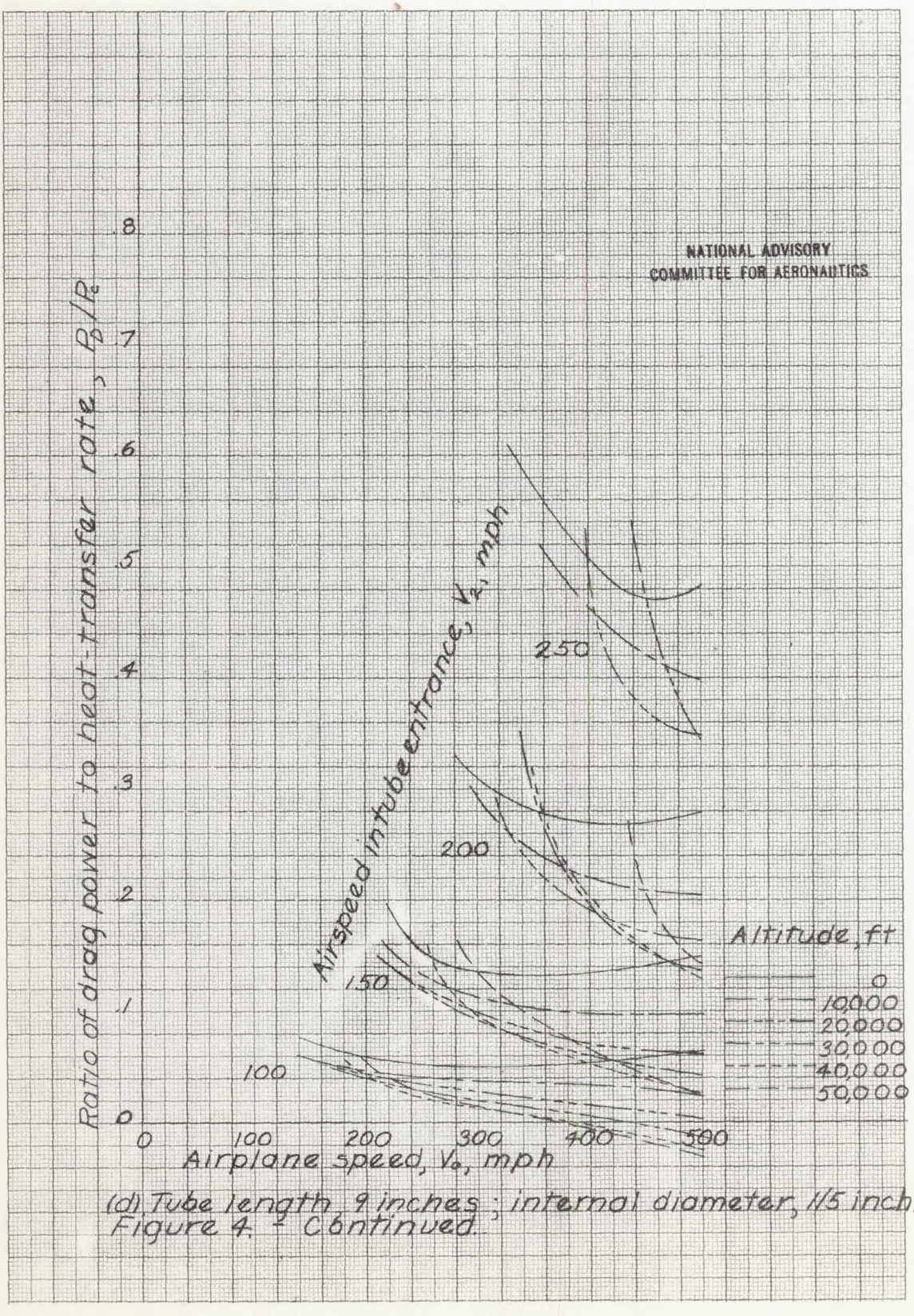

(d) Tube length, 9 inches; internal diameter, 1/5 inch.

Figure 4. - Continued.

L-773

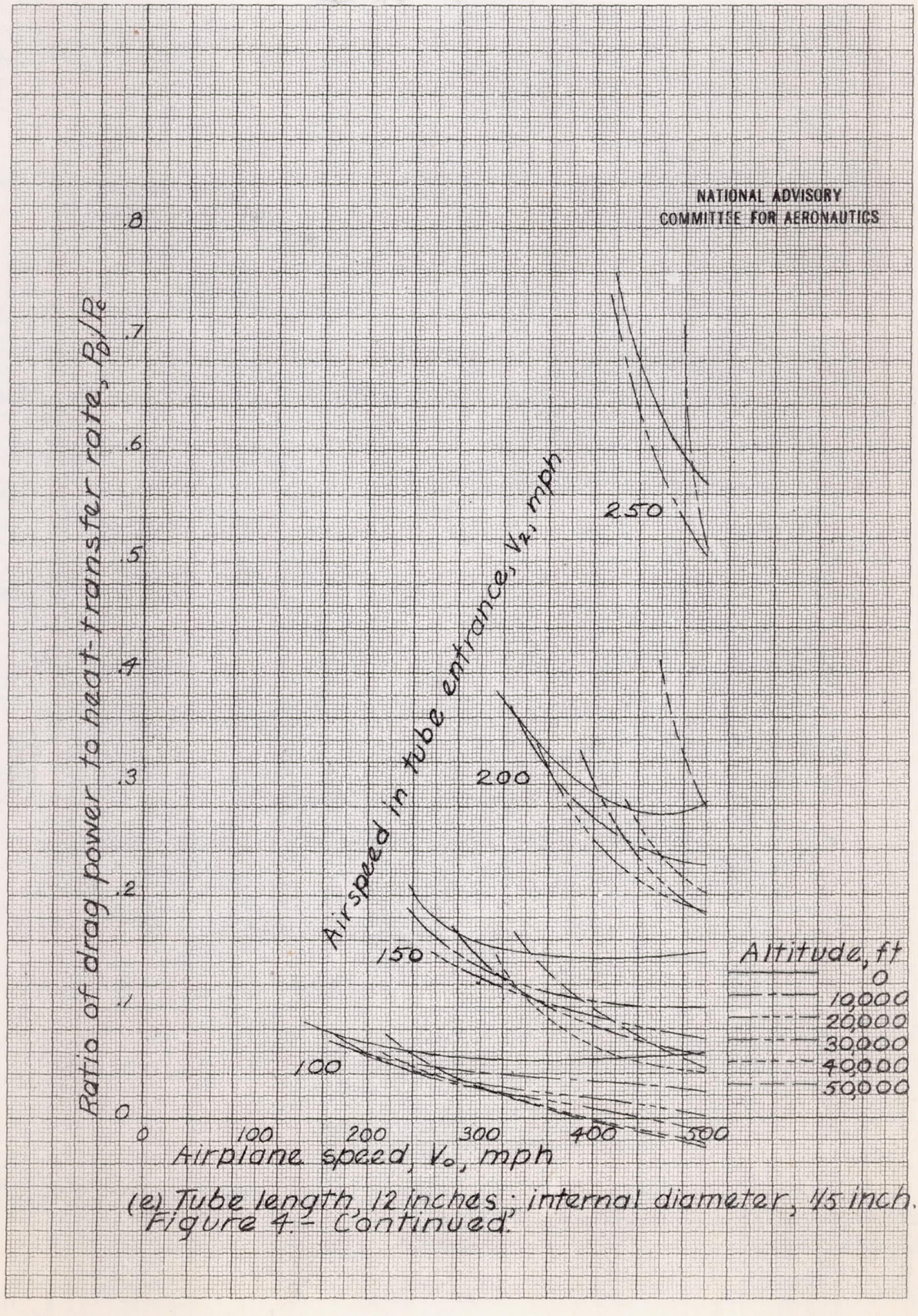

(e) Tube length, 12 inches; internal diameter, 1/5 inch.

Figure 4.- Continued.

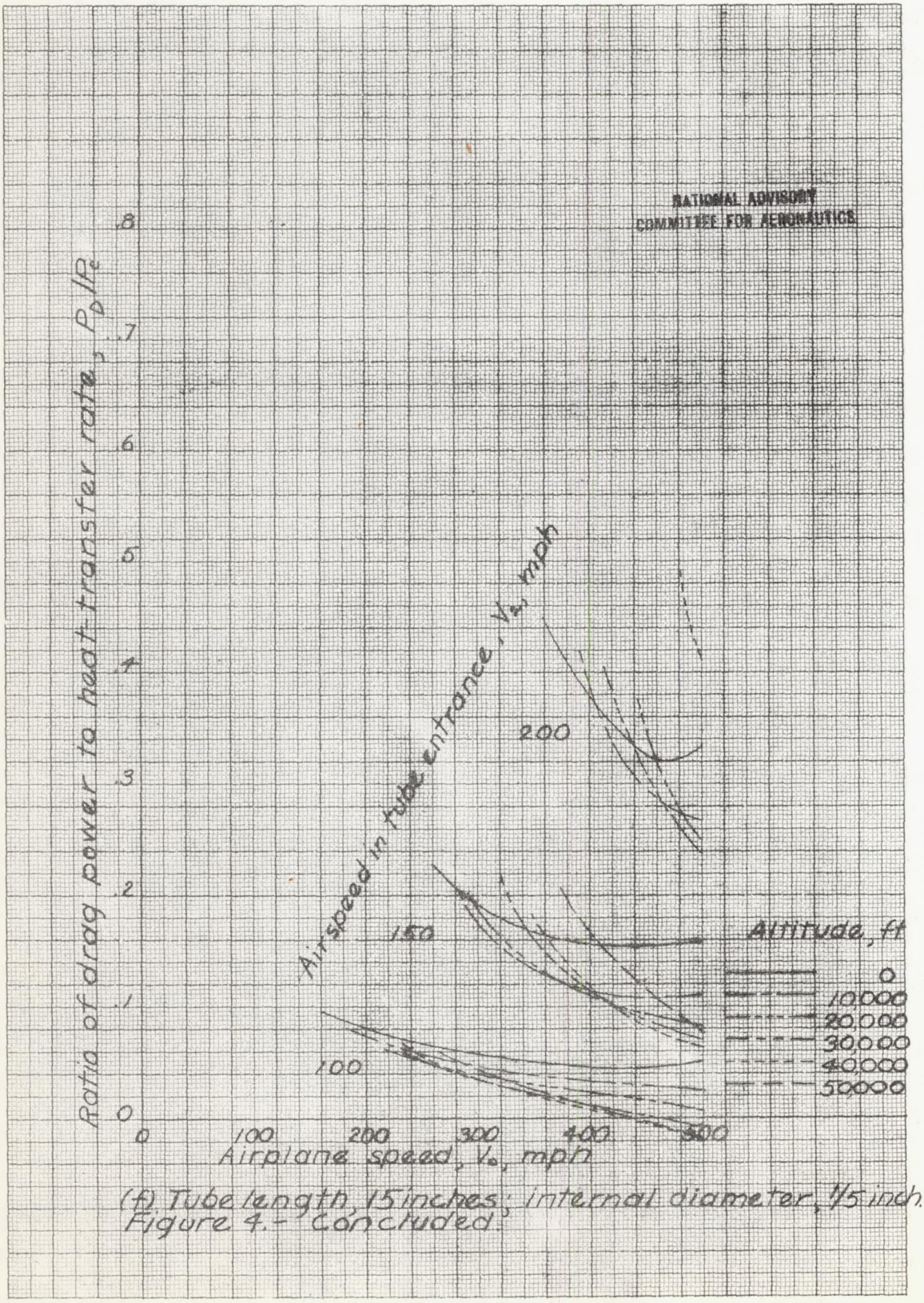

(f) Tube length, 15 inches; internal diameter, 1/5 inch.

Figure 4.- Concluded.